Published in final edited form as:
Phys Med Biol. 2013 June 21; 58(12): 4137–4156. doi:10.1088/0031-9155/58/12/4137.

Interplay effects in proton scanning for lung: A 4D Monte Carlo study assessing the impact of tumor and beam delivery parameters

S Dowdell[1], **C Grassberger**[1,2], **G C Sharp**[1], and **H Paganetti**[1]
S Dowdell: sdowdell@partners.org

[1]Department of Radiation Oncology, Massachusetts General Hospital & Harvard Medical School, Boston MA 02114 [2]Centre for Proton Radiotherapy, Paul Scherrer Institut, 5232 Villigen-PSI, Switzerland

Abstract

Relative motion between a tumor and a scanning proton beam results in a degradation of the dose distribution (interplay effect). This study investigates the relationship between beam scanning parameters and the interplay effect, with the goal of finding parameters that minimize interplay. 4D Monte Carlo simulations of pencil beam scanning proton therapy treatments were performed using the 4DCT geometry of 5 lung cancer patients of varying tumor size (50.4–167.1cc) and motion amplitude (2.9–30.1mm). Treatments were planned assuming delivery in 35×2.5Gy(RBE) fractions.

The spot size, time to change the beam energy (τ_{es}), time required for magnet settling (τ_{ss}), initial breathing phase, spot spacing, scanning direction, scanning speed, beam current and patient breathing period were varied for each of the 5 patients. Simulations were performed for a single fraction and an approximation of conventional fractionation.

For the patients considered, the interplay effect could not be predicted using the superior-inferior (SI) motion amplitude alone. Larger spot sizes (σ ~9–16mm) were less susceptible to interplay, giving an equivalent uniform dose (EUD) of 99.0±4.4% (1 standard deviation) in a single fraction compared to 86.1±13.1% for smaller spots (σ ~2–4mm). The smaller spot sizes gave EUD values as low as 65.3% of the prescription dose in a single fraction. Reducing the spot spacing improved the target dose homogeneity. The initial breathing phase can have a significant effect on the interplay, particularly for shorter delivery times. No clear benefit was evident when scanning either parallel or perpendicular to the predominant axis of motion. Longer breathing periods decreased the EUD. In general, longer delivery times led to lower interplay effects. Conventional fractionation showed significant improvement in terms of interplay, giving a EUD of at least 84.7% and 100.0% of the prescription dose for the small and larger spot sizes respectively.

The interplay effect is highly patient specific, depending on the motion amplitude, tumor location and the delivery parameters. Large degradations of the dose distribution in a single fraction were observed, but improved significantly using conventional fractionation.

Keywords

interplay effect; proton therapy; beam scanning

1. Introduction

The most advanced delivery method of proton therapy currently available is active scanning, which offers several potential benefits over double scattering (Goitein 1983; Pedroni et al. 2005). The inherent flexibility in scanning means that the dose can be conformed to both proximal and distal edges without the use patient-specific hardware (Kooy et al. 2010). Advanced delivery techniques such as on-line adaptive treatments and intensity modulated proton therapy (IMPT) (Lomax et al. 2001) are only possible using scanning.

Double scattering fields are less susceptible to motion than scanning fields, as the entire double scattering field is essentially delivered simultaneously through the use of scatterers and a range-modulator wheel. Scanning treatment fields are typically delivered as a series of iso-energy layers, commencing with the layer of greatest depth (highest energy) and concluding with the shallowest (lowest energy). Two perpendicular magnetic fields are used to scan the beam laterally over the target within each of these layers. The beam energy is varied to conform the dose in depth. The time required to perform this change is termed the energy switching time (τ_{es}). This energy change can be performed directly at the source, for synchrotron based facilities, or using an energy selection system, for cyclotron based systems.

This study focuses on spot scanning (Pedroni et al. 2005), not continuous scanning. In spot scanning, each iso-energy layer is delivered in a series of discrete spots. After the prescribed number of protons has been delivered in a given spot, the scanning magnets are used to reconfigure the system to deliver dose in the subsequent position. This is not an instantaneous process and moving the beam too quickly will result in a position overshoot, causing the spot to be delivered in an incorrect location. Sufficient time must be given to allow the magnets to settle to ensure accurate dose delivery (within a tolerance threshold). This time required for settling, termed the spot settling time (τ_{ss}), is dependent on both the properties of the magnets and the positional accuracy required, with a higher accuracy requiring a longer τ_{ss}.

In the presence of motion, lateral conformity to the target volume cannot be guaranteed (Phillips et al. 1992; Seco et al. 2009). Unlike photons, protons are also sensitive to motion along the beam path and changes in the water equivalent path length due to their finite range (Goitein 1983; Mori et al. 2008; Pedroni et al. 2005). Furthermore, the delivery method of scanning fields makes them inherently sensitive to motion because in addition to the motion of the tumor, the beam itself is also moving during delivery. It is this relative motion between the beam and tumor, termed the interplay effect (Kooy et al. 2010; Bortfeld et al. 2002), which is the focus of this study. The interplay of the proton beam and the tumor motion leads to tumor sub-volumes either being under or over-dosed. This has clinical implications as the minimum dose delivered to the tumor volume has been previously shown to correlate with the probability of local control (Lomax et al. 2001; Tomé & Fowler 2002).

The interplay effect has been extensively studied for various photon radiotherapy techniques such as IMRT (Pedroni et al. 2005; Bortfeld et al. 2002; Berbeco et al. 2006), Tomotherapy (Phillips et al. 1992; Sterpin et al. 2012; Seco et al. 2009), RapidArc (Ong et al. 2011) and VMAT (Rao et al. 2012). The general consensus from these previous studies is that the interplay effect is insignificant for fractionated photon techniques, as any variations induced average out over the course of a conventionally fractionated treatment.

A previous study (Lambert et al. 2005) concluded that proton scanning techniques should not be used for targets with motion greater than 10mm. More recent results have demonstrated that scanning may be a feasible treatment option in the presence of motion up to 20mm, depending on the spot size and treatment configuration (Grassberger et al. 2013).

Much of the previous work in motion during proton scanning treatments has focused on repainting strategies (Zenklusen et al. 2010; Bassler et al. 2010; Seco et al. 2009) or different treatment sites such as liver (Knopf et al. 2011).

In this study, simulated proton treatments were delivered to 4DCT scans of lung cancer patients to quantify the interplay effect using Monte Carlo simulations. We applied Monte Carlo simulations because analytical algorithms are expected to have significant uncertainties in proton therapy {Paganetti:2012ct}. They neglect the position of inhomogeneities relative to the Bragg peak depth (Urie et al. 1984) and cannot accurately predict range degradation arising from multiple Coulomb scattering due to their insensitivity to complex geometries and density variations (Urie et al. 1986). Previous work has also demonstrated the differences between analytical and Monte Carlo methods (Paganetti et al. 2008; Paganetti 2012).

The detailed time structure of the field is considered and time dependent parameters are varied across a range of values relevant to currently operating proton facilities to determine any change the choice or restriction of these parameters may have on the interplay effect.

2. Method

2.1. Patients

This study was performed using CT data from 5 patients. The patients were selected to cover the range of motion amplitudes likely to be observed in a clinical setting. Whilst the average SI motion of a larger patient cohort will be lower (Sonke & Belderbos 2010; Seppenwoolde et al. 2002), the aim of this study is to investigate interplay effects for patients with a wide range of motion amplitudes. The relevant characteristics of the patients in this study are shown in table 1.

2.2. Treatment planning

All treatment plans were generated using ASTROID (Kooy et al. 2010), an in-house treatment planning system (TPS) used at Massachusetts General Hospital for proton beam scanning. The IGTV was defined such that it encompassed the GTV in all 10 phases of the 4DCT. The CTV was defined as the GTV with a 8mm uniform margin to account for microscopic disease, with the ICTV defined to cover the CTV in all 4DCT phases. A conventional PTV was defined, as the ICTV with a uniform 5mm margin, to account for potential uncertainties in patient setup and beam delivery.

Treatment planning was performed on the average intensity-projection (IP) CT, with IGTV filled with HU50, based on the methodology of Kang *et al* (Kang et al. 2007). The prescription dose for all plans was 87.5Gy(RBE), delivered to the ICTV in 2.5Gy(RBE)/fraction. The prescription dose and fractionation regime chosen is in accordance with the previous study of Chang *et al* (Chang et al. 2011) and with an ongoing clinical trial (ClinicalTrials.gov ID: NCT00495040). The treatment plan was accepted if ≥99% of the ICTV and ≥95% of the PTV received the prescription dose. Multi-criteria optimization (MCO) (Chen et al. 2010) was used to reduce the dose to normal tissue as much as possible. All plans used 2 spot scanning fields with the field-specific target inhomogeneity restricted to <20%. The beam angles were chosen to minimize mean lung dose (MLD) and the volume of lung receiving 20Gy(RBE) (V_{20}). The recommendation of V_{20} <30–35% made in the QUANTEC report (Marks et al. 2010) was satisfied by all treatment plans for all 5 patients.

The mean dose in a scanning proton field will vary based on spot size and spacing. For a static treatment plan, smaller spot sizes are typically able to provide a sharper fall-off at high doses in the dose-volume histogram. The same holds true when the spot spacing is reduced.

The same planning constraints were used in all plans which will inherently lead to a lower required mean dose for smaller spot sizes and spot spacing values to achieve the required target dose constraints.

2.3. Monte Carlo simulations

2.3.1. TOPAS—All Monte Carlo simulations were performed using TOPAS (TOol for PArticle Simulation) (Perl et al. 2012). TOPAS is layered upon the Geant4 Monte Carlo toolkit (Agostinelli et al. 2003). TOPAS version a9 and Geant4 version 4.9.5 were used in this work. TOPAS has been benchmarked against measured depth dose profiles and 2D dose profiles, absolute dosimetry measurements and for measurements of the beam delivery time structure (Testa et al. 2013). TOPAS simulations were generally within clinical tolerances and will be used for future quality assurance and beam commissioning simulations at our institution.

2.3.2. MCAUTO—An automated suite of scripts, MCAUTO, is implemented at our institution to handle data transfer between the treatment planning system and TOPAS. It automatically configures TOPAS based on the selection of patient and treatment planning information and is connected to the departmental patient and treatment planning database. MCAUTO retrieves the fluence maps from the TPS for each of the fields in the simulation. For typical treatment sites, the time structure of the beam delivery does not need to be taken into account when performing the dose calculation.

For this study we developed an additional 4D version of MCAUTO (MCAUTO-4D). It considers the time at which each spot in the field will be delivered based on the hardware properties of the beam delivery system. The quantities considered in the timing calculation include the τ_{es}, τ_{ss} time, the speed at which the beam is laterally scanned, the beam current and the patient breathing period. The breathing period of each of the patients was considered and the 4DCT itself was then handled as 10 individual static CT scans, each having a time window of a fraction of that period. Each of the parameters included in the timing calculation are customizable and can be adapted to reflect the properties of a different facility or different breathing characteristics.

Based on the treatment parameters and the time at which each spot is delivered, MCAUTO-4D calculates the corresponding phase of the 4DCT in which each spot would be delivered. The TOPAS input files are then generated based on the results of this timing. This leads to 10 individual simulations, each on an individual phase of the 4DCT, with the number of protons, their lateral position and energy being time dependent.

2.3.3. Deformable image registration—To perform the deformable image registration (DIR) of the resulting dose distributions, an in-house developed tool, Plastimatch, was used (http://plastimatch.org). End of exhale (T_{50}) was used as the reference phase for the DIR, due its stability and reproducibility. Thus, all quantities reported are for the CTV after the dose distributions of each phase have been warped to the 50% phase (CTV-50).

A number of different algorithms are available in Plastimatch, however we chose to use the B-spline as it has been tested most rigorously (Shackleford et al. 2010; Sharp et al. 2010). The high density contrast between lung tumors and the surrounding tissue means any uncertainty introduced by deformable image registration algorithm will likely be less than 2mm (Brock 2010).

2.4. Studied parameter space

2.4.1. Spot size—For each patient, simulations were generated for 2 different energy dependent (70–230MeV) pencil beam spot sizes, termed BigSpots (σ ~9–16mm) and SmallSpots (σ ~2–4mm) respectively. These spot sizes reflect the current extremes used in clinical proton scanning treatments at various institutions and will give the limits of interplay that can be expected. A medium spot size was not included as we did not have access to the relevant clinical beam data the results yielded would lie within the limits obtained from the BigSpots and SmallSpots.

2.4.2. Energy switching time (τ_{es})—For each spot size, 3 different times to change the beam energy in-between layers were simulated, i.e. τ_{es} of 0.08s, 1s and 3s were included in the parameter space. The fastest reported τ_{es} in the literature is 0.08s achieved at the Paul Scherrer Institut (PSI) (Pedroni et al. 2011). The other values were chosen to cover the range of values likely to be encountered at other facilities, including Massachusetts General Hospital (MGH).

2.4.3. Spot settling time (τ_{ss})—Due to the variability in inter-facility hardware, the spot settling (τ_{ss}) time differs depending on the scanning hardware, i.e. the scanning magnets. Thus, τ_{ss} values of 1ms, 5ms and 10ms were simulated. Combining these values with the τ_{es} values led to 9 different parameter combinations per patient.

2.4.4. Spot spacing—The spot spacing can typically be chosen as a free parameter in the treatment planning program. The default spot spacing for all simulations in this study was 0.7σ, with σ being the spot size. To assess the impact of spot spacing on the interplay effect, simulations were repeated for all combinations of τ_{es} and τ_{ss} and for BigSpots with the spot spacing changed to 0.5σ and 0.3σ. Altering the spot spacing changes the time structure of the field, as a smaller spot spacing will require a higher number of spots and thus will increase the number of times that τ_{ss} will be invoked during the field delivery. Increased overlap of adjacent spots should make the field less susceptible to motion effects at the expense of increased delivery time.

2.4.5. Scanning direction—The scanning pattern used at our institution consists of a zigzag pattern in each iso-energy layer, with the longer axis parallel to the fast scanning direction to minimize the delivery time. Depending on the motion direction, altering the scanning direction may make the field less susceptible to motion and interplay effects. Whether this can be done depends on the flexibility of the treatment control system at a given facility. The default scanning direction in this study was to have the long axis parallel to the superior-inferior (SI) axis of motion.

Typically, scanning systems employ two magnets to move the beam laterally. The configuration of these magnets and their position in the treatment head can lead to a difference in scanning speed in the two lateral directions. This is the case at both MGH and at PSI (Zenklusen et al. 2010).

The beam orientation relative to the predominant axis of motion is important in interplay studies (Lambert et al. 2005; Grözinger et al. 2006; Bert & Durante 2011). It can be expected that the amount of interplay will vary if the tumor motion is parallel or orthogonal to the fast scanning direction. To assess the impact of the scanning direction, the different τ_{es}, τ_{ss} and phase values were simulated for BigSpots and SmallSpots with a spot spacing of 0.7σ, with the fast scanning axis changed to be orthogonal to the SI axis. This required a change in the timing of the fields as the spot ordering becomes different when scanning in a different direction.

2.4.6. Scanning speed—The lateral scanning speed defines the time taken to move the beam from one spot position to the next. It is momentum dependent and thus varies within a single field, so we quote the maximum speed, which occurs for the minimum deliverable proton energy. The lateral scanning speed was varied to determine any effect this had on the interplay due to changes in the time spent in each iso-energy layer.

The default setup for all simulations was to have the fast magnet scan parallel to the SI axis with a maximum speed of 30m/s. The slow magnet thus scans perpendicular to the SI axis, with a maximum speed of 3m/s. These values are close to those encountered at MGH. The fast magnet was adjusted to have maximum scanning speeds of 20m/s and 40m/s with the slow magnet set to 2m/s and 4m/s.

2.4.7. Beam current—The rate at which dose can be deposited effects the time to deliver the field. The time required to deposit the dose in a spot, in seconds, is given by equation 1.

$$time = \frac{number\ of\ protons \times q}{beam\ current} \quad (1)$$

where $q = 1.6 \times 10^{-19}$C and the beam current is in Amperes. The default beam current for all simulations was set to a typical value of 2nA. The beam current was changed from 2nA to 1nA and 5nA to observe any change in interplay effect based on the dose deposition rate. For these simulations, only 2.5Gy(RBE) per fraction was considered. For other fractionation regimes, e.g. hypofractionation, and doses per fraction, the number of protons within each spot will vary due to the different dose per fraction, which thus alters the time structure of the field.

2.4.8. Initial breathing phase—For each of the 9 combinations of τ_{es} and τ_{ss}, and for each of the 5 patients, 4 different initial breathing phases were considered. Evenly spaced initial phases of 0% (peak inhale), 25% (mid-exhale), 50% (peak exhale) and 75% (mid-inhale) were simulated. The 2 fields within a given treatment plan were both started at the same initial phase. The point at which scanning commences within the breathing cycle may be significant, given the majority of the total dose in a scanning field is deposited in the distal layer. For shorter treatment times, especially those close to the duration of a single breathing cycle, the initial phase may be even more critical.

2.4.9. Breathing period—The default breathing period in this study was 5s, which has also been used in previous studies assessing 4D radiotherapy (e.g. (Knopf et al. 2011; Grassberger et al. 2013; Zhang et al. 2012)). To determine the changes in interplay due to a different breathing period, simulations were performed for BigSpots using a τ_{es}=0.08s, τ_{ss}=1ms and a spot spacing of 0.7σ for different breathing periods. Breathing periods of 4.0s, 4.5s, 5.0s, 5.5s and 6.0s were simulated by adjusting the time spent in each phase of the original 4DCT.

2.5. Approximation of fractionation

When respiratory gating is not used, the initial phase of a given fraction will essentially be random. As the number of fractions increases, the distribution of initial phases will approach a uniform distribution. A conventionally fractionated treatment is approximated in this work by the superposition and normalization of the 4 dose distributions with initial phases of 0%, 25%, 50% and 75%. The resulting dose distribution is denoted as *n-fx*.

The method for generating the *n-fx* dose distribution is identical when the treatment parameters are varied. However, the approximation loses some validity if a significantly

smaller number of fractions are used, as the distribution of initial breathing phases will not necessarily be even.

2.6. Analysis of the interplay effect

A number of different metrics were chosen to analyze the interplay effect. The mean dose in the CTV-50 is used to determine whether dosimetric effects are indeed due to interplay. The total energy deposited, and hence mean dose, within the tumor should remain close to constant given the ITV-based planning approach employed. A loss in mean dose means the beam is not irradiating part of the tumor volume for a period of the breathing cycle. This may be either due to the tumor moving out of the beam path, motion induced range changes or a geometric misalignment of the beam. If the mean dose remains constant, any effect observed within the target is purely due to interplay.

The minimum and maximum doses within the target were also acquired to show the degradation of the dose distribution due to interplay. A potential issue with using maximum and minimum dose is these quantities will be observed in a single voxel of the CT scan and are inherently sensitive to the statistics of the Monte Carlo simulations. Minimum dose in particular is of paramount importance, as it is known to correlate with the probability of local control (Tomé & Fowler 2002). D_1 and D_{99} are used as surrogates for maximum and minimum doses respectively throughout this study to make the results less sensitive to statistics.

Another method of quantifying the dose distribution degradation is to analyze the homogeneity. This can be assessed using quantities such as D_5-D_{95}, D_2-D_{98} and D_1-D_{99}. Previous studies (Knopf et al. 2011; Grassberger et al. 2013) have used similar quantities to quantify the interplay effect.

The volumes receiving 95% (V_{95}), 100% (V_{100}) and 105% (V_{105}) of the prescription dose were also quantified. V_{95} can be used to determine the amount of under dosage as previously employed in the study of Bert *et al* (Bert et al. 2008).

Finally, the equivalent uniform dose (EUD) (Niemierko 1997) was calculated for each of the dose distributions. Given that interplay effects reduce the homogeneity in the dose distribution, using the EUD provides insight into the clinical significance.

3. Results and Discussion

The prescription dose for all treatment plans in this study was 87.5Gy(RBE), delivered in 2.5Gy(RBE) fractions. Different facilities and protocols may operate using alternative fractionation schemes and prescription doses, so all results are presented as percentages of the prescription dose rather than absolute dose values.

The lung doses vary slightly due to the different treatment plans that were required for different spot sizes and spot spacing values for each of the 5 patients. However for all different treatment configurations based on the same treatment plan, the variation in the lung V_5 and V_{20} is less than 1%. The consistency of the lung doses demonstrates that all changes in the target dose distributions are due to interplay.

Unless specified otherwise, all results are reported for a single fraction and relative to the default settings shown in Table 2. The default scanning direction was parallel to the SI axis.

3.1. Spot size

Figure 1 shows the interplay metrics assuming a single fraction treatment for patient 1. The values are the averages obtained from the 36 combinations of τ_{es}, τ_{ss} and initial phase, with the error bars equal to ±1 standard deviation.

SmallSpots shows both higher maximum and lower minimum doses compared to BigSpots. This leads to a less homogeneous dose distribution as shown in figure 1(b). The EUD (figure 1(c)) perhaps best illustrates the differences between the two considered spot sizes, with BigSpots yielding an average EUD of 93.7%, compared to 65.3% for SmallSpots.

Figure 2 shows the interplay metrics for patient 2 assuming a single fraction. Dose homogeneity is improved using BigSpots, with a D_1-D_{99} of 26.7% compared to 37.2% for SmallSpots. BigSpots gives an average EUD of 103.4% compared to 97.9% for SmallSpots. The EUD values for both spot sizes are higher for patient 2 compared to patient 1, perhaps due to the smaller motion amplitude.

The data for a single fraction for patient 3 is displayed in figure 3. In similarity to the other patients, SmallSpots gives a higher maximum dose and lower minimum dose on average, leading to poorer dose homogeneity compared to BigSpots. Despite the increased motion amplitude for patient 3, the average EUD values are higher than those observed for patient 2 for both BigSpots (103.5%) and SmallSpots (99.0%).

Patient 4 is the only patient in the study that shows a lower average maximum dose for SmallSpots. The primary tumor for patient 4 is located on the inferior and lateral lung wall and is largely surrounded by soft tissue, rather than lung tissue and is close to a rib. This location reduces the accuracy of the image registration compared to the other patients. This could be partially responsible for similar results for the two spot sizes for this patient despite the relatively large SI motion amplitude.

The homogeneity metrics (see figure 4(b)) show similar values for both spot sizes. The dose distributions are very similar as illustrated by the similar EUD values. BigSpots still result in a higher EUD of 100.9% compared to 98.9% for SmallSpots. This average EUD difference of 2% is the smallest difference among the 5 patients considered and is much lower than the 28.4% difference observed for patient 1.

Finally, figure 5 shows the interplay metrics for patient 5. Despite the comparatively low SI motion amplitude of 2.9mm, patient 5 exhibits a higher degree of interplay compared to patient 4. The D_1-D_{99} for SmallSpots (37.1%) is close to twice as high as the 20.5% obtained for BigSpots. The average EUD value for BigSpots is 100.7% compared to 92.5% for the SmallSpots even with the comparatively small motion amplitude.

For all patients, the minimum (D_{99}) dose is always lower for SmallSpots and the maximum (D_1) is higher for 4 out of 5 patients. Target dose homogeneity is improved with BigSpots and a lower average EUD is observed for all 5 patients for SmallSpots. These results are in agreement with previous studies which have shown a larger spot size gives improved CTV coverage (Bert & Durante 2011).

3.2. Energy switching time (τ_{es})

The Spearman rank correlation was calculated between τ_{es} and each of the interplay metrics for every plan simulated when predominantly scanning parallel to the SI axis. No significant correlations ($p<0.05$) were observed between any of the metrics and either spot size when the spot spacing was 0.7σ. For the BigSpots with 0.5σ, a significant correlation was observed between τ_{es} and EUD, D_1-D_{99}, D_2-D_{98}, V_{95} and D_{99}. When the spacing was

reduced to 0.3σ, τ_{es} showed significant correlation with EUD, D_1-D_{99}, D_2-D_{98}, D_5-D_{95}, V_{95} and D_{99}. Increasing τ_{es} reduces the EUD, target dose homogeneity and the minimum dose. These results justify the use of multiple homogeneity measures. If only D_5-D_{95} was used, the conclusion would be reached that τ_{es} had no significant impact on dose homogeneity for BigSpots with 0.5σ spacing, whilst the correlations with D_1-D_{99} and D_2-D_{98} suggest otherwise.

3.3. Spot settling time (τ_{ss})

The Spearman rank correlations between τ_{ss} and each of the interplay metrics were also calculated for all simulated plans when predominantly scanning parallel to the SI axis. τ_{ss} essentially determines how much time is spent in each iso-energy layer during the irradiation.

For the BigSpots with 0.7σ, τ_{ss} significantly correlated with D_5-D_{95}. For the 0.5σ spacing significant correlations were observed between τ_{ss} and D_1-D_{99}, D_2-D_{98}, D_5-D_{95}, D_1 and D_{99}. The only significant correlation observed for BigSpots with a spacing of 0.3σ was a decreasing D_1 with increasing τ_{ss}. For SmallSpots with 0.7σ spacing, τ_{ss} showed significant correlation with D_1-D_{99} and D_2-D_{98}. Longer values of τ_{ss} gave improved dose homogeneity.

3.4. Spot spacing

Figure 6 shows the results for the different spot spacing values for BigSpots. Reducing the spot spacing increases the delivery time due to the increased number of spots and hence the number of times τ_{ss} is encountered. A narrower spot spacing is able to provide a more conformal 3D plan, which leads to a slight decrease in the mean dose. Decreasing the spot spacing reduces the maximum dose and the minimum dose increases, which gives a more homogeneous dose distribution as shown in figure 6(b). This is however achieved at the cost of increased treatment time. The treatment time varies markedly depending on the treatment parameters. For example, with BigSpots and a spot spacing of 0.7σ, the delivery time varied between 7.2s and 46.8s for patient 1 when the delivery parameters where changed. For the same set of delivery parameters, decreasing the spot spacing from 0.7σ to 0.5σ results in a delivery time approximately twice as long. Further decreasing the spacing to 0.3σ results in a delivery time ~5.5 times longer than the delivery time for 0.7σ. For each of the 5 patients, the change in EUD is <1% when reducing the spot spacing from 0.7σ to 0.5σ and 0.3σ, despite the observed increase in homogeneity.

Similar results have been previously observed by Bert *et al* (Bert et al. 2009) and a reduced spot spacing both laterally and in depth has been proposed for treatments with significant motion at the Heidelberg Ion Beam Therapy Center.

3.5. Scanning direction

Changing the predominant scanning axis from parallel to the SI axis to perpendicular showed no clear trends for the two different spot sizes. The change in the dose distribution based on the scanning direction is highly influenced by the other delivery parameters, with no clear trend observed in terms of τ_{es}, τ_{ss} or initial breathing phase. For some configurations, the EUD is higher when predominantly scanning parallel to the SI axis, whilst for others it is higher when predominantly scanning perpendicular to it. Table 3 shows the mean EUD difference and range when scanning parallel and perpendicular to the SI axis for the 5 patients for BigSpots and SmallSpots with 0.7σ spacing.

By taking the average values shown in Table 3, one could reach the conclusion that the scanning direction is not critical, particularly for BigSpots. However, this is not necessarily

the case as the difference in EUD can be up to 8.7%, whilst for SmallSpots the EUD difference can be as high as 29.1%.

These results somewhat contradict those previously reported by Lambert *et al* (Lambert et al. 2005) and Grözinger *et al* (Grözinger et al. 2006) who reported more severe underdosage when scanning was perpendicular to the motion direction in a simplified geometry. Lambert *et al* used ray tracing to perform their dose calculation in a box-shaped target in a homogeneous water phantom that moved with a constant velocity in 1 dimension. Additionally, Lambert *et al* compared scanning in iso-energy layers to scanning in depth (see figures 2 and 3 in (Lambert et al. 2005)). The previous study of Grözinger (Grözinger et al. 2006) used a 60mm diameter sphere in a homogeneous medium and was performed assuming raster scanning for Carbon-ion therapy. Raster scanning differs from spot scanning in that settling time (i.e. τ_{ss}) is not invoked multiple times during the irradiation of each iso-energy layer. Thus, the time required to deliver a field using raster scanning is shorter than spot scanning, particularly for the SmallSpots fields, which contain approximately 10 times as many spots as the BigSpots fields. The time required to deliver a proton field for all configurations in this study for all patients is at least 10s, which corresponds to 2 nominal breathing cycles. Averaging effects are thus likely to occur, which may reduce the significance of the scanning direction, particularly when the delivery time is further increased.

In contrast to the previous studies, this work uses real patient geometry and motion trajectories obtained directly from 4DCT data. The patient geometry is heterogeneous and tumor motion is not unidirectional or constant velocity. Respiratory motion is typically quoted in the SI direction, however target motion can be up to 5mm in the AP and LR directions (Langen & Jones 2001), possibly higher. Thus, the effects of changing the scanning direction will not be as large for a real patient tumor trajectory as has been previously observed in previous studies that assumed unidirectional motion.

3.6. Scanning speed

Altering the scanning speed made no significant changes to the dose distributions. For all parameter configurations for each of the 5 patients, the total time required for moving the beam during the irradiation is less than 0.5s. Any change to the scanning speed within the range considered makes little difference in terms of the time structure of the proton field and thus has minimal effect on the interplay effect. Any observed changes in the interplay metrics were less than 1%. To induce a notable change in the dose distribution, the scanning speed would likely have to be altered by at least an order of magnitude.

3.7. Beam current

As demonstrated in equation 1, the beam current essentially dictates how quickly the dose can be deposited in each spot throughout the irradiation. Any alterations to the beam current will show greatest effect for the shortest treatment times. The only significant correlation ($p<0.001$) observed was a decrease in the dose homogeneity (D_1-D_{99}, D_2-D_{98} and D_5-D_{95}) with increasing beam current. Increasing the beam current, reduces the target dose homogeneity, as averaging effects, which typically reduce interplay, cannot occur when the fields are delivered on the order of a single breathing cycle.

Depositing the dose faster for the considered configurations led to more significant interplay. Only with a beam current of 5nA was it possible to achieve beam delivery times of approximately a single breathing cycle (5s) for the patients included in this study. Such delivery times have been previously shown to give the highest amount of interplay (Zenklusen et al. 2010). This is an important consideration, as increasing the capabilities of

the hardware (e.g. higher beam current) may in fact reduce the quality of some treatments in terms of interplay.

The beam current was assumed constant throughout each of the fields. The majority of dose in a scanning field is deposited in the few most distal layers. Applying a variable beam current will result in minimal changes in delivery time for the most distal layers due to the small changes in current for adjacent layer energies. For the more proximal layers, the significantly lower spot weights mean that a difference in beam current will have minimal impact on the spot delivery time. Simulation of a variable beam current may be required for intensity-modulated proton therapy fields where more proximal layers can contain high spot weights.

3.8. Initial breathing phase

Figure 8 shows how the EUD, mean target dose, dose homogeneity and V_{95} vary when the initial breathing phase is altered. The values in the figures show the wide variation in the considered metrics when the delivery parameters are altered, as demonstrated by relatively large error bar size.

Significant correlations were observed between the initial breathing phase and V_{95}, V_{100}, V_{105}, D_1, D_{99}, mean dose and EUD for BigSpots with a spot spacing of 0.7σ. The importance of the initial phase is highlighted by the fact that this is the only variable which showed a significant correlation with the mean target dose. The spots in the distal layers deposit the majority of the dose in each field. Altering the initial breathing phase causes these high weight spots to be delivered while the tumor is at a different position. The largest effects in mean dose were observed for the shortest delivery times where averaging effects are not as prevalent.

Despite the significant correlations, there were no distinct trends, as shown in Figure 7. For a given set of parameters there was typically an initial breathing phase that gave the highest mean dose, however this optimal phase changed when the parameters were varied.

When the spacing was reduced to 0.5σ significant correlations were observed between the initial phase and V_{95}, D_{99} and EUD. No significant correlations were observed when the spacing was reduced further to 0.3σ for the BigSpots. For the SmallSpots with a spacing of 0.7σ, the initial phase shows significant correlation with D_1-D_{99} and D_2-D_{98}.

Bert *et al* (Bert et al. 2008) also observed significant changes in dose coverage based on the initial phase, with some phases leading to coverage similar to the static reference plan whilst others showed over 50% underdosage to the CTV.

3.9. Breathing period

All previous results presented assumed a constant breathing period of 5s. By varying the breathing period in 0.5s steps from 4.0s–6.0s it was observed that longer breathing periods lead to a reduction in target dose homogeneity. Significant correlations ($p<0.001$) were observed between the breathing period and D_1-D_{99}, D_2-D_{98} and D_5-D_{95}. No significant correlations were observed with any of the other variables and breathing period.

The largest effect from changing the breathing period would likely be observed for the shortest delivery time. This occurs for patient 1 with a τ_{es} of 0.08s τ_{ss} of 1ms using BigSpots and a spot spacing of 0.7σ. For this case, the 4.0s breathing period gave the highest average single fraction EUD of 91.4% (range: 82.2%–106.8%) whilst the 6.0s period gave the lowest of 86.6% (range: 63.8%–102.9%). The minimum EUD observed in any of the 4 initial breathing phases increased when the breathing period was shortened.

The breathing period itself will be most significant for short treatment times. It is well established that patients do not breath with a constant 5s period. In a clinical irradiation, which will typically cover multiple breathing periods, the varying breathing period of the patient will further smear out the dose distribution, additionally reducing any effects from interplay.

3.10. Fractionation

By combining the dose distributions from the 4 evenly spaced initial phases, we obtained an approximation of a conventionally fractionated treatment. For all parameters and treatment configurations considered, no significant correlations are observed when considering a treatment in n fractions (where $n = 35$ here). Despite the interplay effects observed in each single fraction of a conventionally fractionated treatment regime, if the initial phase space is approximately evenly sampled over the treatment course, the interplay effects are reduced, yielding a more conformal overall dose distribution than is observed for any individual fraction.

Table 4 shows the average EUD values and ranges for the *n-fx* dose distributions for the BigSpots and SmallSpots with a spot spacing of 0.7σ. The average is taken over the 9 different τ_{es} and τ_{ss} combinations for each of the 5 patients.

For BigSpots, all combinations of parameter settings result in an *n-fx* EUD of at least 100% of the prescription dose. The mean *n-fx* EUDs for 0.5σ and 0.3σ for the BigSpots are within 1% of the "total" value for 0.7σ shown in Table 3. The range of individual *n-fx* values is wider for both 0.5σ (7.2%) and 0.3σ (6.3%) compared to the 3% for 0.7σ spacing. This suggests the benefit observed by reducing the spot spacing when examining the single fraction case is diminished and potentially negligible when using conventional fractionation.

For the SmallSpots, the *n-fx* EUD is higher for all patients than the single fraction EUD, however only patients 4 and 5 give an *n-fx* EUD greater than the prescription dose. For patient 1, which has as 30.6mm motion amplitude and shows the highest interplay, the *n-fx* EUD for SmallSpots is 87.5%, an improvement of 22.2% compared to the average single fraction. These results demonstrate that conventional fractionation reduces the interplay effect and leads to an improved target dose distribution. But the example of patient 1 shows that, in particular with small spot sizes, conventional fractionation can still experience significant interplay effects.

For hypofractionated treatments, the higher doses per fraction will alter the time structure of the field due to the increased time required to deposit the dose in each spot. The lower number of fractions also means that the distribution of initial breathing phases may not be evenly sampled which means the approximation used here for conventional fractionation may no longer be valid.

5. Conclusion

The interplay effect is highly patient specific, depending on the motion amplitude, tumor location and the delivery parameters of the field. Note that this study assumed treatment without gating and beam delivery without "re-painting". Both aspects will be incorporated in future studies.

Larger spot sizes are less susceptible to interplay effects. Decreasing the time required to change the beam energy resulted in an improved EUD and target dose homogeneity. Increasing the spot settling time, and hence the time spent in each iso-energy layer, also improved the target dose homogeneity. Changing the initial breathing phase can have a

significant effect on the target mean dose, homogeneity and EUD, particularly for shorter beam delivery times. Reducing the spacing between adjacent spots makes the plan less susceptible to interplay and improves the target dose homogeneity. Changing the predominant scanning direction alters the dose distribution, with the effect being highly dependent on the delivery parameters. Varying the scanning speed over the range considered here had negligible effect on the interplay. Shorter breathing periods showed higher EUD values and increasing the beam current reduced the dose homogeneity. The *n-fx* approximation of fractionation showed significant improvement in terms of interplay. For BigSpots and SmallSpots, the *n-fx* EUD was at least 100.0% and 84.7% of the prescription dose respectively, regardless of the delivery parameters. In general, altering the treatment parameters to increase the delivery time reduced the interplay.

Acknowledgments

This work was funded by NCI grant CA111590.

The authors would like to thank Partners Research Computing, particularly Jon Jackson, for maintenance of the computing cluster.

References

Agostinelli S, et al. Geant4—a simulation toolkit. Nuclear Instruments and Methods in Physics Research Section A: Accelerators, Spectrometers, Detectors and Associated Equipment. 2003; 506(3):250–303.

Bassler N, et al. Dose- and LET-painting with particle therapy. Acta Oncologica. 2010; 49(7):1170–1176. [PubMed: 20831510]

Berbeco RI, Pope CJ, Jiang SB. Measurement of the interplay effect in lung IMRT treatment using EDR2 films. Journal of Applied Clinical Medical Physics. 2006; 7(4)

Bert C, Durante M. Motion in radiotherapy: particle therapy. Physics in Medicine and Biology. 2011; 56(16):R113–R144. [PubMed: 21775795]

Bert C, et al. Gated Irradiation With Scanned Particle Beams. International Journal of Radiation Oncology, Biology, Physics. 2009

Bert C, Grözinger SO, Rietzel E. Quantification of interplay effects of scanned particle beams and moving targets. Physics in Medicine and Biology. 2008; 53(9):2253–2265. [PubMed: 18401063]

Bortfeld T, et al. Effects of intra-fraction motion on IMRT dose delivery: statistical analysis and simulation. Physics in Medicine and Biology. 2002; 47(13):2203–2220. [PubMed: 12164582]

Brock KK. Results of a Multi-Institution Deformable Registration Accuracy Study (MIDRAS). International Journal of Radiation Oncology, Biology, Physics. 2010; 76(2):583–596.

Chang JY, et al. Toxicity and patterns of failure of adaptive/ablative proton therapy for early-stage, medically inoperable non-small cell lung cancer. International Journal of Radiation Oncology, Biology, Physics. 2011; 80(5):1350–1357.

Chen W, et al. A fast optimization algorithm for multicriteria intensity modulated proton therapy planning. Medical Physics. 2010; 37(9):4938–4945. [PubMed: 20964213]

Goitein M. Beam scanning for heavy charged particle radiotherapy. Medical Physics. 1983; 10(6): 831–840. [PubMed: 6318060]

Grassberger C, et al. Motion Interplay as a Function of Patient Parameters and Spot Size in Spot Scanning Proton Therapy for Lung Cancer. International Journal of Radiation Oncology, Biology, Physics. 2013 in press.

Grözinger SO, et al. Simulations to design an online motion compensation system for scanned particle beams. Physics in Medicine and Biology. 2006; 51:3517–3531. [PubMed: 16825746]

Kang Y, et al. 4D Proton treatment planning strategy for mobile lung tumors. International Journal of Radiation Oncology, Biology, Physics. 2007; 67(3):906–914.

Knopf A-C, Hong TS, Lomax A. Scanned proton radiotherapy for mobile targets—the effectiveness of re-scanning in the context of different treatment planning approaches and for different motion characteristics. Physics in Medicine and Biology. 2011; 56(22):7257–7271. [PubMed: 22037710]

Kooy H, et al. A Case Study in Proton Pencil-Beam Scanning Delivery. International Journal of Radiation Oncology, Biology, Physics. 2010; 76(2):624–630.

Lambert J, et al. Intrafractional motion during proton beam scanning. Physics in Medicine and Biology. 2005; 50(20):4853–4862. [PubMed: 16204877]

Langen KM, Jones DTL. Organ motion and its management. International Journal of Radiation Oncology, Biology, Physics. 2001; 50(1):265–278.

Lomax AJ, et al. Intensity modulated proton therapy: A clinical example. Medical Physics. 2001; 28(3):317–324. [PubMed: 11318312]

Marks LB, et al. Radiation Dose–Volume Effects in the Lung. International Journal of Radiation Oncology, Biology, Physics. 2010; 76(3):S70–S76.

Mori S, et al. Quantitative Assessment of Range Fluctuations in Charged Particle Lung Irradiation. International Journal of Radiation Oncology, Biology, Physics. 2008; 70(1):253–261.

Niemierko A. Reporting and analyzing dose distributions: A concept of equivalent uniform dose. Medical Physics. 1997; 24(1):103–110. [PubMed: 9029544]

Ong C, Verbakel W, Cuijpers J. Dosimetric Impact of Interplay Effect on RapidArc Lung Stereotactic Treatment Delivery. International Journal of Radiation Oncology, Biology, Physics. 2011; 79:305–311.

Paganetti H. Range uncertainties in proton therapy and the role of Monte Carlo simulations. Physics in Medicine and Biology. 2012; 57(11):R99–R117. [PubMed: 22571913]

Paganetti H, et al. Clinical implementation of full Monte Carlo dose calculation in proton beam therapy. Physics in Medicine and Biology. 2008; 53(17):4825–4853. [PubMed: 18701772]

Pedroni E, et al. Experimental characterization and physical modelling of the dose distribution of scanned proton pencil beams. Physics in Medicine and Biology. 2005; 50(3):541–561. [PubMed: 15773729]

Pedroni E, et al. Pencil beam characteristics of the next-generation proton scanning gantry of PSI: design issues and initial commissioning results. The European Physical Journal Plus. 2011; 126(7)

Perl J, et al. TOPAS: An innovative proton Monte Carlo platform for research and clinical applications. Medical Physics. 2012; 39(11):6818–6837. [PubMed: 23127075]

Phillips MH, et al. Effects of respiratory motion on dose uniformity with a charged particle scanning method. Physics in Medicine and Biology. 1992; 37(1):223–234. [PubMed: 1311106]

Rao M, et al. Dosimetric Impact of Breathing Motion in Lung Stereotactic Body Radiotherapy Treatment Using Image-Modulated Radiotherapy and Volumetric Modulated Arc Therapy. International Journal of Radiation Oncology, Biology, Physics. 2012; 83:e251–e256.

Seco J, et al. Breathing interplay effects during proton beam scanning: simulation and statistical analysis. Physics in Medicine and Biology. 2009; 54(14):N283–N294. [PubMed: 19550002]

Seppenwoolde Y, Shirato H, Kitamura K. Precise and real-time measurement of 3D tumor motion in lung due to breathing and heartbeat, measured during radiotherapy. International Journal of Radiation Oncology, Biology, Physics. 2002; 53(4):822–834.

Shackleford JA, Kandasamy N, Sharp GC. On developing B-spline registration algorithms for multi-core processors. Physics in Medicine and Biology. 2010; 55:6329–6351. [PubMed: 20938071]

Sharp GC, et al. Evaluation of plastimatch B-Spline registration on the EMPIRE10 data set. Medical Image Analysis for the Clinic: A Grand Challenge, MICCAI 2010. 2010

Sonke J-J, Belderbos J. Adaptive radiotherapy for lung cancer. Seminars in Radiation Oncology. 2010; 20(2):94–106. [PubMed: 20219547]

Sterpin E, et al. Helical tomotherapy for SIB and hypo-fractionated treatments in lung carcinomas: A 4D Monte Carlo treatment planning study. Radiotherapy and Oncology. 2012

Testa M, et al. Experimental validation of the TOPAS Monte Carlo system for proton therapy applications. Physics in Medicine and Biology. 2013 under submission.

Tomé WA, Fowler JF. On cold spots in tumor subvolumes. Medical Physics. 2002; 29(7):1590–1598. [PubMed: 12148742]

Urie M, et al. Degradation of the Bragg peak due to inhomogeneities. Physics in Medicine and Biology. 1986; 31(1):1–15. [PubMed: 3952143]

Urie M, Goitein M, Wagner M. Compensating for heterogeneities in proton radiation therapy. Physics in Medicine and Biology. 1984; 29(5):553–566. [PubMed: 6330772]

Zenklusen SM, Pedroni E, Meer D. A study on repainting strategies for treating moderately moving targets with proton pencil beam scanning at the new Gantry 2 at PSI. Physics in Medicine and Biology. 2010; 55(17):5103–5121. [PubMed: 20702927]

Zhang Y, et al. Respiratory liver motion estimation and its effect on scanned proton beam therapy. Physics in Medicine and Biology. 2012; 57(7):1779–1795. [PubMed: 22407290]

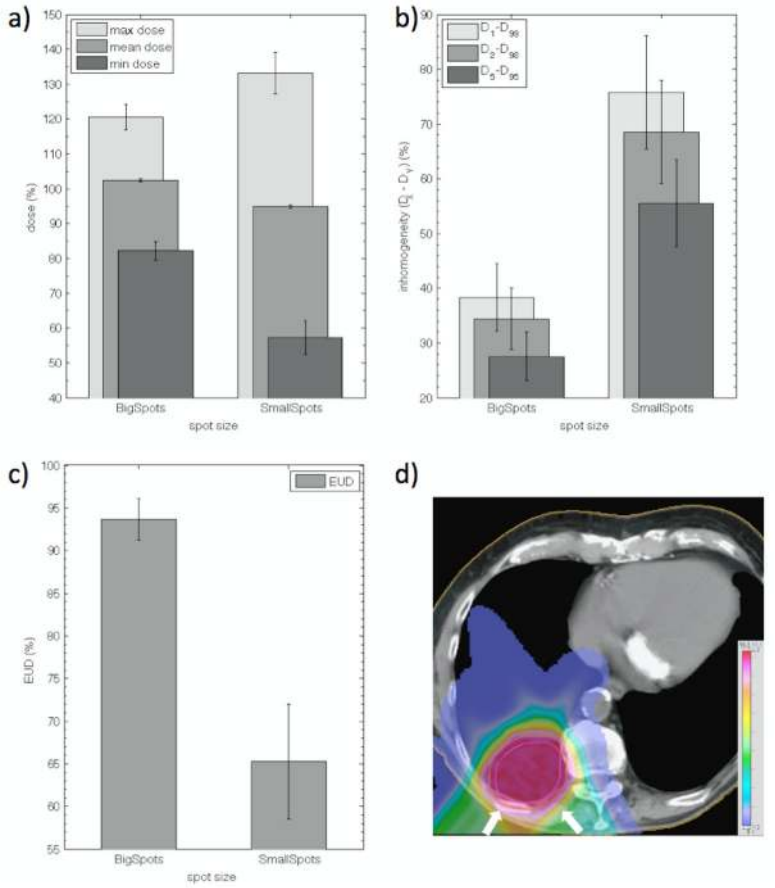

Figure 1.

Average of the various interplay metrics for a single fraction for patient 1 for BigSpots and SmallSpots with a spot spacing of 0.7σ. The values are the averages of the results from the 36 combinations of τ_{es}, τ_{ss} and phase. The error bars are ±1 standard deviation. (a) shows the maximum (D_1), mean and minimum (D_{99}) doses, (b) shows the dose homogeneity: D_1-D_{99}, D_2-D_{98} and D_5-D_{95}, (c) shows the EUD and (d) shows the planned dose distribution for SmallSpots. The contours shown are the ICTV and the PTV, with the white arrows indicating the field directions and the color bar units in Gy(RBE).

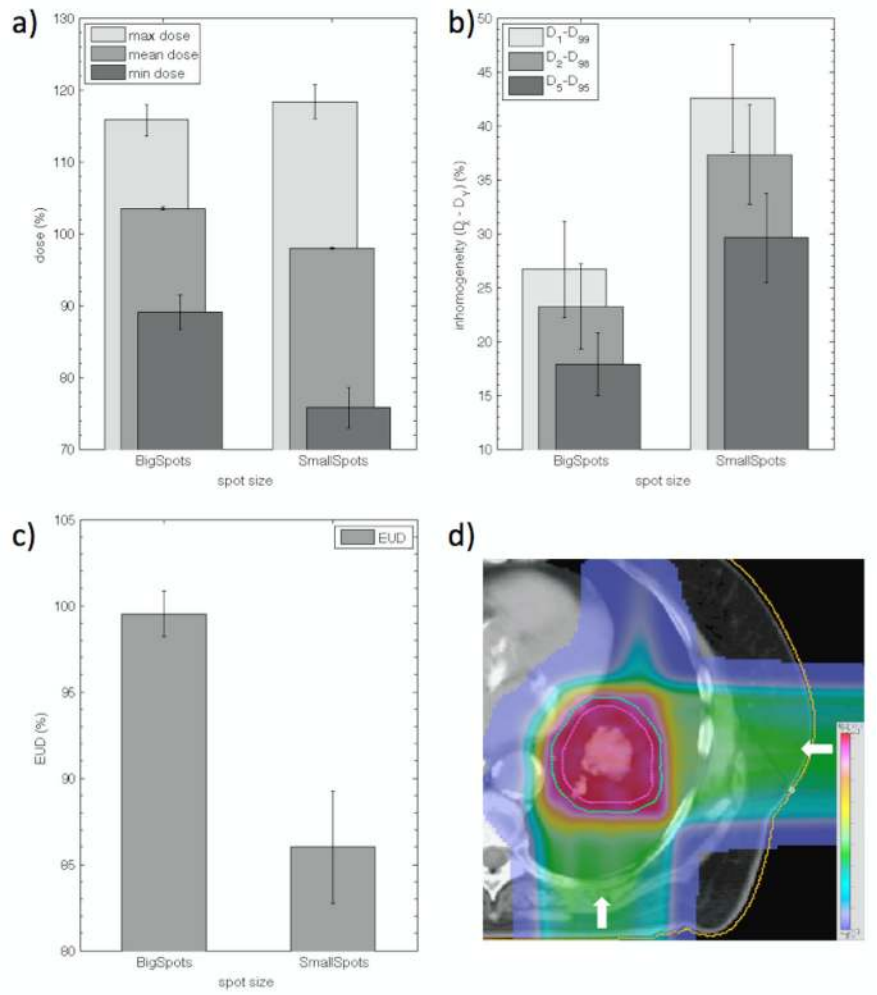

Figure 2.

Average of the various interplay metrics for a single fraction for patient 2 for BigSpots and SmallSpots with a spot spacing of 0.7σ. The values are the averages of the results from the 36 combinations of τ_{es}, τ_{ss} and phase. The error bars are ±1 standard deviation. (a) shows the maximum (D_1), mean and minimum (D_{99}) doses, (b) shows the dose homogeneity: D_1-D_{99}, D_2-D_{98} and D_5-D_{95}, (c) shows the EUD and (d) shows the planned dose distribution for SmallSpots. The contours shown are the ICTV and the PTV, with the white arrows indicating the field directions and the color bar units in Gy(RBE).

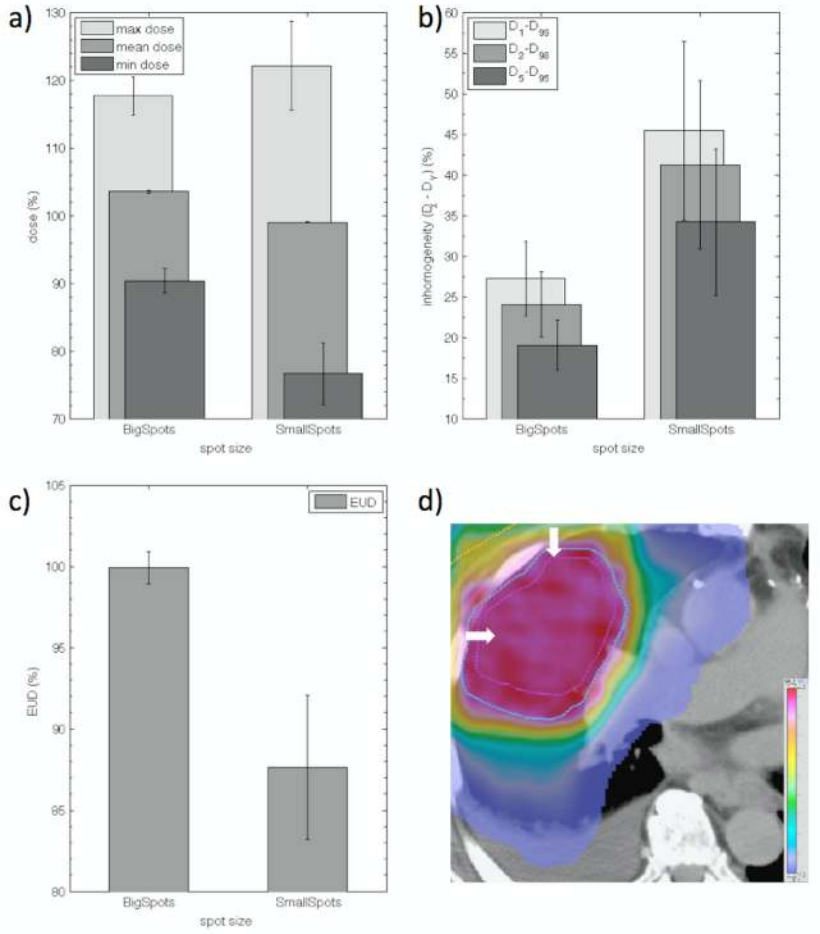

Figure 3.

Average of the various interplay metrics for a single fraction for patient 3 for BigSpots and SmallSpots with a spot spacing of 0.7σ. The values are the averages of the results from the 36 combinations of τ_{es}, τ_{ss} and phase. The error bars are ±1 standard deviation. (a) shows the maximum (D_1), mean and minimum (D_{99}) doses, (b) shows the dose homogeneity: D_1-D_{99}, D_2-D_{98} and D_5-D_{95}, (c) shows the EUD and (d) shows the planned dose distribution for SmallSpots. The contours shown are the ICTV and the PTV, with the white arrows indicating the field directions and the color bar units in Gy(RBE).

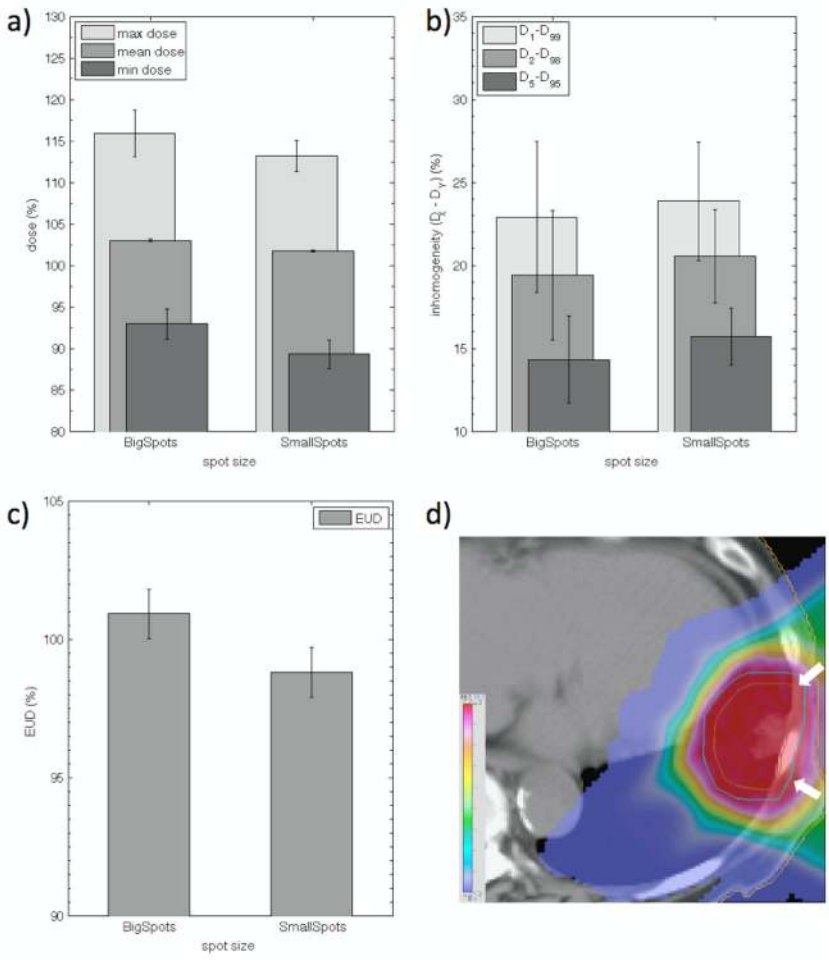

Figure 4.

Average of the various interplay metrics for a single fraction for patient 4 for BigSpots and SmallSpots with a spot spacing of 0.7σ. The values are the averages of the results from the 36 combinations of τ_{es}, τ_{ss} and phase. The error bars are ±1 standard deviation. (a) shows the maximum (D_1), mean and minimum (D_{99}) doses, (b) shows the dose homogeneity: D_1-D_{99}, D_2-D_{98} and D_5-D_{95}, (c) shows the EUD and (d) shows the planned dose distribution for SmallSpots. The contours shown are the ICTV and the PTV, with the white arrows indicating the field directions and the color bar units in Gy(RBE).

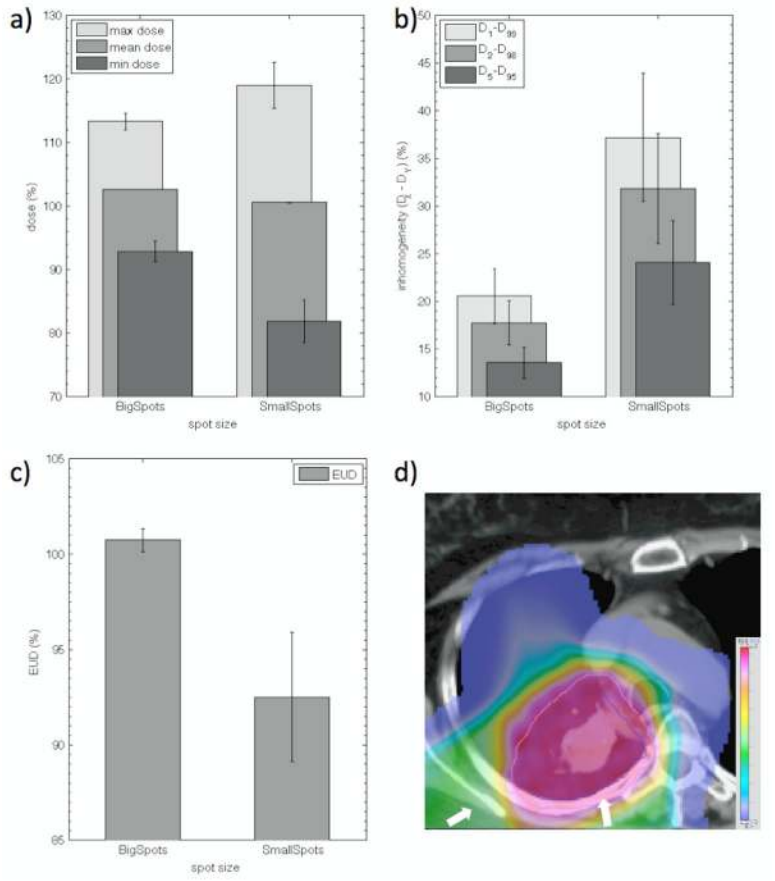

Figure 5.

Average of the various interplay metrics for a single fraction for patient 5 for BigSpots and SmallSpots with a spot spacing of 0.7σ. The values are the averages of the results from the 36 combinations of τ_{es}, τ_{ss} and phase. The error bars are ±1 standard deviation. (a) shows the maximum (D_1), mean and minimum (D_{99}) doses, (b) shows the dose homogeneity: D_1-D_{99}, D_2-D_{98} and D_5-D_{95}, (c) shows the EUD and (d) shows the planned dose distribution for SmallSpots. The contours shown are the ICTV and the PTV, with the white arrows indicating the field directions and the color bar units in Gy(RBE).

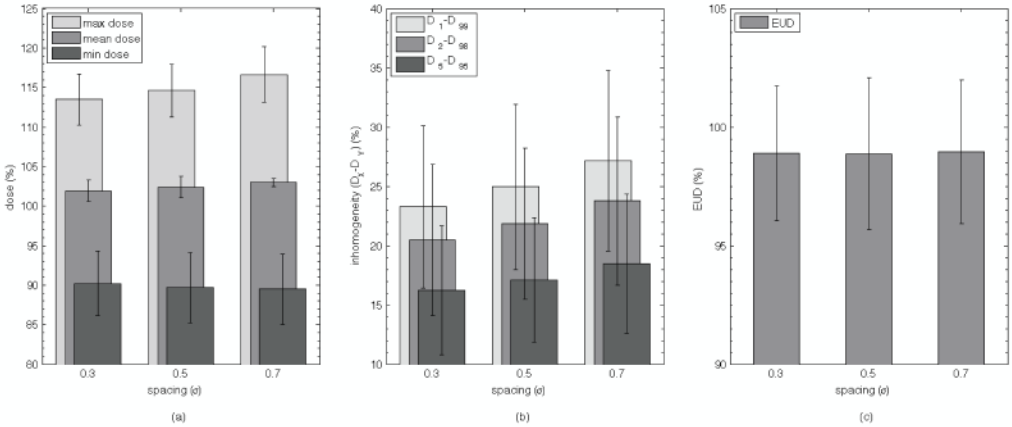

Figure 6.

Average of the various interplay metrics in a single fraction for the 5 patients included in the study for BigSpots with a spot spacing of 0.3σ, 0.5σ and 0.7σ. The values are the averages of the results from the 36 combinations of τ_{es}, τ_{ss} and phase for all 5 patients. The error bars are ±1 standard deviation. (a) shows the maximum (D_1), mean and minimum (D_{99}) doses, (b) shows the dose homogeneity: D_1-D_{99}, D_2-D_{98} and D_5-D_{95} and (c) shows the EUD.

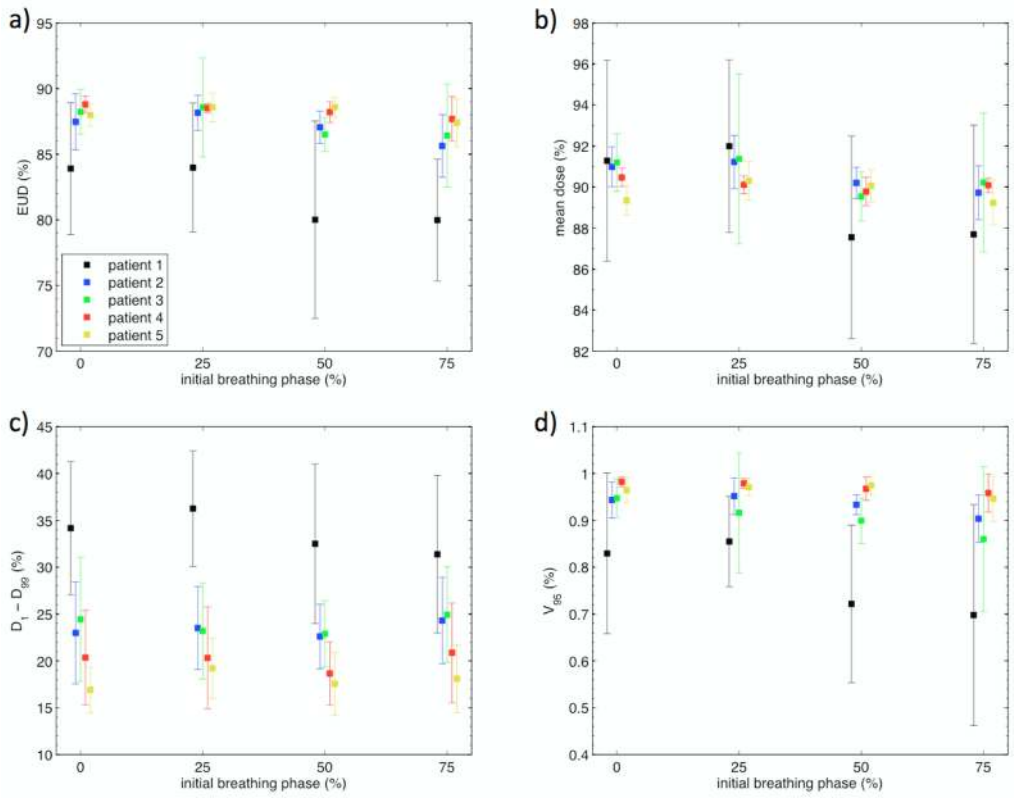

Figure 7.

Variations in EUD (a), mean target dose (b), D_1-D_{99} (c) and V_{95} (d) with changing initial breathing phase for the 5 patients for BigSpots with 0.7σ lateral spot spacing. All values are in percentage of prescribed dose and are the averages of the 9 combinations of τ_{es} and τ_{ss}. The error bars are ±1 standard deviation. The values are slightly offset in the x-axis for improved clarity.

Table 1

Details of the 5 patients included in the study. The peak-to-peak motion amplitude along the superior-inferior axis is shown along with the volumes of the CTV at peak exhale (CTV-50) and the ICTV.

Patient	Motion amplitude [mm]	CTV-50 volume [cc]	ICTV volume [cc]
1	30.6	73.7	118.3
2	10.7	83.3	132.5
3	20.2	167.1	255.7
4	15.1	50.4	71.3
5	2.9	104.7	109.2

Table 2

Default values for the different parameters in the Monte Carlo simulations. The 4 initial phases were simulated in all cases. The max scanning speed is for the fast magnet, with the slow magnet shown in parentheses.

Parameter [unit]	default value
τ_{es} [s]	0.08
τ_{ss} [ms]	1
spot spacing [σ]	0.7
breathing period [s]	5.0
beam current [nA]	2
max scanning speed [m/s]	30 (3)

Table 3

Average difference in EUD (scanning parallel to SI axis - scanning perpendicular to SI axis) for BigSpots and SmallSpots with spacing 0.7σ. The values are averaged over the 36 combinations of τ_{es}, τ_{ss} and initial phase for each patient. The range of values is shown in parentheses.

patient	BigSpots (%)	SmallSpots (%)
1	− 0.8 (−6.6–8.7)	−0.0 (−1.3–1.4)
2	0.2 (−3.2–2.7)	−4.8 (−29.1–10.4)
3	0.2 (−3.9–5.6)	−3.0 (−16.3–4.9)
4	−0.1 (−0.9–1.3)	−0.4 (−4.7–2.9)
5	0.1 (−1.8–1.4)	−3.2 (−14.2–16.5)

Table 4

Average EUD values for the *n-fx* dose distributions for the 5 patients. The range of EUD values are given in parentheses. All values are percentages of the prescription dose.

patient	BigSpots (%)	SmallSpots (%)
1	100.5 (100.0–101.4)	87.5 (84.7–89.1)
2	102.7 (102.3–103.0)	96.3 (95.7–96.6)
3	102.8 (102.5–102.9)	97.7 (97.6–97.9)
4	102.7 (102.6–102.9)	101.6 (101.4–101.7)
5	102.2 (101.1–102.3)	100.0 (100.0–100.1)
total	102.2 (100.0–103.0)	96.6 (84.7–101.7)